Numerical investigation of the aerodynamics and wake structures of horizontal axis wind turbines by using nonlinear vortex lattice method

Hakjin Lee and Duck-Joo Lee*

Korea Advanced Institute of Science and Technology (KAIST), Daejeon 34141, Republic of Korea

Abstract

Wind turbines are emerging as one of the most promising and cost-effective renewable energy sources, due to their economical merits and technical maturity. It is important to accurately predict the aerodynamic performance of rotor blades for efficient design of wind turbine. Among the various numerical approaches, the vortex lattice method (VLM) is one of the most suitable models for wind turbine aerodynamics because the wind turbine mostly operates in the subsonic flow. However, it inherently cannot predict the nonlinear aerodynamic characteristics at a high angle of attack. In the current paper, a nonlinear vortex lattice method (NVLM) has been suggested to extend the existing VLM for handling the nonlinear stall and post-stall behaviors. This can be possible by finding a control point in the airfoil where the effective angle of attack is applied. This paper mainly discusses the development and validation of the NVLM for predicting the aerodynamic performances and the wake geometry against the measurements on the MEXICO rotor model. The comparison results show that the aerodynamic loads and tip vortex trajectories computed by NVLM are in significantly good agreement with the measured data. In addition, the complicated and unsteady wake structures are also analyzed using vortex particle method.

Keywords: Horizontal axis wind turbines; Wind turbine aerodynamics; Wind turbine wake; Vortex particle method; Vortex lattice method; Nonlinear vortex lattice method

* Corresponding author. KAIST, 291 Daehak-ro, Yuseng-gu, Daejeon 34141, Republic of Korea.
Tel.: +82-42-350-3716; fax: +82-42-350-3710; E-mail: djlee@kaist.ac.kr (Duck-Joo Lee)

1. Introduction

Accurately predicting the aerodynamic loads acting on rotor blades is significantly important for the efficient and reliable design of wind turbine that can minimize the cost of energy. Many studies have been devoted to developing the aerodynamic models for wind turbines that can evaluate the aerodynamic performance and help analyze an underlying flow field around rotor blades. Among various aerodynamic models, such as blade element momentum (BEM) theory and computational fluid dynamics (CFD) methods, vortex methods can accurately predict the aerodynamic loads acting on the rotor blades of the wind turbine, and can describe the vorticity fields without the numerical dissipation error. These models bridge the gap in fidelity between BEM and CFD. Vortex methods can provide more accurate solutions than BEM methods, and require less computing time and resources than CFD methods. However, the major shortcoming of vortex methods is that the flow phenomena arising from the viscous and compressible effects cannot be inherently captured since they are based on the assumption of incompressible potential flow. Especially vortex methods are not able to predict the nonlinear aerodynamic behaviors in the stall and post-stall regions, thus incurring in excessively over-predicted results. Therefore, novel and complementary approaches are needed to overcome the limitations of the existing methods.

There have been attempts to predict the stall and post-stall characteristics occurring at a high angle of attack using vortex methods. Anderson et al. [1] and Owens [2] used the nonlinear lift line method (LLM) and Weissinger nonlinear lifting line method (Weissinger-LLM) to study the aerodynamic behavior of the finite wings at the post-stall conditions. They predicted the lift and drag coefficients of the straight rectangular and swept-back wings, respectively, and the results were compared against the measurements. Their results showed that the nonlinear LLM solutions at high angle of attack well matched with experimental data. Gupta and Leishman [3, 4] and Duque et al. [5] conducted the performance prediction of a horizontal-axis wind turbine ex posed to the attached and stalled flow conditions using nonlinear LLM. They can calculate the unsteady aerodynamic loads acting on the wind turbine blades, even if the flow separation occurs from the upper surface of the rotor blades due to the high wind speed. In addition, van Garrel [6] and Gaertner [7] developed the nonlinear LLM with vortex strength correction for the aerodynamic analysis of wind turbine blades. Airfoil look-up tables are consulted to provide the sectional aerodynamic coefficients at the spanwise positions as a function of local inflow velocity and effective angle of attack. The strength of bound vortices on the rotor blades are iteratively corrected by using the sectional lift coefficients obtained from the airfoil table. However, the evident limitation of the LLM and Weissinger's LLM is that the three-dimensional rotor geometry and various blade planforms could not be sufficiently represented by only a single chordwise vortex element. It is not enough to accurately model the modern wind turbine blades.

Meanwhile, lifting surface method, referred to as vortex lattice method (VLM) can well represent the various geometries of the rotor blade, including camber, curvature, sweep angles, since the vortex elements are placed on the actual camber surface of the rotor blades in the chordwise and spanwise directions. The various methodologies for handling the nonlinear aerodynamic behavior applied to the VLM have been also suggested. Mukherjee and Gopalarathnam [8], and Gopalarathnam and Segawa [9] developed the decambering approach that used the deviation between the nonlinear lift curve and the potential linear lift curve to correct the local effective angle of attack. Compared to the experiments, they accurately predicted the post-stall aerodynamic characteristics of the finite wings. However, Hosangadi et al. [10] pointed out that the corrected results have been found to be quite inaccurate when the deviation becomes significant at high angles of attack or deep stall condition. Santos and Marques [11] proposed the pre- and post-stall correction approach based on the Kirchhoff flow model which is employed to define a separation point function. According to the value of the separation point in the airfoils, the aerodynamic influence coefficients are directly corrected to take account of the stall effects. For application to wind turbines, Abedi et al. [12] developed the enhanced VLM with free-wake model that is coupled with a tabulated airfoil data to consider the stall and viscous effects. The angle of attack is modified based on VLM solutions and airfoil data, and it is used to obtain the sectional lift and drag forces at the radial positions. In addition, Kim et al. [13] suggested the nonlinear vortex strength correction method that is incorporated with airfoil look-up table and bound vortex correction. However, nonlinear system of equations have to be solved by an optimization algorithm to correct the vortex strength each time step, and it may cause the computational burden and convergence problems.

In order to obtain the accurate coefficients from airfoil table, it is important to carefully define the location of the control point where the effective angle of attack is evaluated. However, the previous studies did not explicitly deal with the crucial issues related to the location of the control points. In the present research, nonlinear vortex lattice method (NVLM) is suggested to predict the aerodynamic loads on wind turbine blades exposed to the attached and stalled flow conditions. NVLM is supplemented with the airfoil look-up table and iterative circulation correction to take into account the nonlinear aerodynamic behavior at high angle of attack and viscous phenomena. One of the major feature of the proposed method is that it does not require for solving the nonlinear system of equations and computing the Jacobian matrix that allows for low computational cost. In addition, the mathematical derivation is included to solve the problem of determining the suitable location of the control point.

The main objective of the present study is to elucidate the strategies used for NVLM and validate the model accuracy against the measurements on MEXICO wind turbine under axial flow conditions. The comparison results shows that NVLM can predict the significantly accurate blade loads and wake structures, even if the wind turbine blades experience the flow separation. It indicates that the proposed method is capable of handling the nonlinear aerodynamic behavior occurring at high angle of attack.

2. Nonlinear vortex lattice method

According to the aerodynamic force coefficient conventions for the rotor blade of the wind turbine, all other aerodynamic performance coefficients, such as normal (C_N), tangential (C_A), thrust (C_T) and torque (C_Q), can be evaluated using lift (C_L) and drag (C_D) coefficients in conjunction with their reference angles. The normal and tangential force coefficients are relative to the chord line plane, while the thrust and torque coefficients are relative to the rotation plane, as shown in Fig. 1.

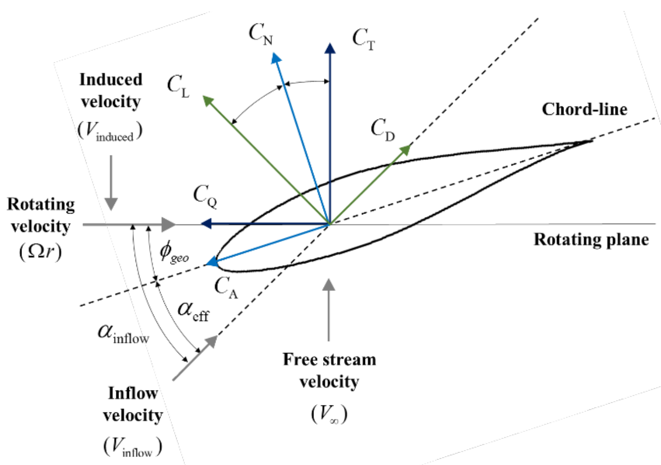

Fig. 1 Aerodynamic force coefficient conventions

$$C_N = C_L \cos(\alpha_{\text{eff}}) + C_D \sin(\alpha_{\text{eff}}) \qquad \text{Eq. (1)}$$

$$C_A = C_L \sin(\alpha_{\text{eff}}) - C_D \cos(\alpha_{\text{eff}}) \qquad \text{Eq. (2)}$$

where C_N and C_A are the normal and tangential force coefficients related to the chord line plane

$$C_T = C_L \cos(\alpha_{\text{infow}}) + C_D \sin(\alpha_{\text{infow}}) \qquad \text{Eq. (3)}$$

$$C_Q = C_L \sin(\alpha_{\text{infow}}) - C_D \cos(\alpha_{\text{infow}}) \qquad \text{Eq. (4)}$$

where C_T and C_Q are the thrust and torque coefficients related to the rotating plane.

The lift and drag coefficients of each blade section rely largely upon the local inflow velocity and effective angle of attack. As shown in Eq. (5), the local inflow velocity at each blade section is composed of the freestream velocity ($\mathbf{V}_\infty$), the rotor rotational velocity ($\mathbf{\Omega} \times \mathbf{r}$), the self-induced velocity ($\mathbf{V}_{\text{ind,bound}}$) and the wake-induced velocity ($\mathbf{V}_{\text{ind,wake}}$). The local inflow velocity ($\mathbf{V}_{\text{inflow}}$) and the effective angle of attack (α_{eff}) can be calculated as follows:

$$\mathbf{V}_{\text{inflow}} = \mathbf{V}_\infty - \mathbf{\Omega} \times \mathbf{r} + \mathbf{V}_{\text{ind,bound}} + \mathbf{V}_{\text{ind,wake}} \qquad \text{Eq. (5)}$$

$$\alpha_{\text{inflow}} = \tan^{-1}\left(\frac{\mathbf{V}_{\text{inflow}} \cdot \mathbf{a}_3}{\mathbf{V}_{\text{inflow}} \cdot \mathbf{a}_1}\right) \qquad \text{Eq. (6)}$$

$$\alpha_{\text{eff}} = \alpha_{\text{inflow}} - \phi_{geo} \qquad \text{Eq. (7)}$$

where α_{inflow} is the local inflow angle and ϕ_{geo} is the local geometric pitch angle including local twist angle and collective pith angle at each blade section. $\mathbf{a}_1$ and $\mathbf{a}_3$ are the unit vectors along tangential and normal directions to the rotating plane, respectively.

2.1 Determination of control point

To incorporate the look-up table in the vortex methods, the control points where an effective angle of attack and local inflow velocity are evaluated for obtaining aerodynamic coefficients should be specified at each blade section. In cases of the LLM or Weissinger's LLM, the collocation points, placed at three-quarters of the chord, are typically used as control points. However, the location of the control point is ambiguous in VLM, since there are *M* collocation points along the chordwise direction. An issue related to the location of control points has been mathematically solved by our coauthor [14]. A concise summary of the determination of control points for a cambered airfoil is provided as follows.

Consider the cambered airfoil that is modeled by M number of vortex elements along the chordwise direction. If the airfoil is assumed to have a parabolic camber distribution as shown in Eq. (8), then the point vortex elements and an arbitrary control point are placed on the camber line. Here x and y are the coordinates of the camber line, δ is the maximum camber, and c is the chord length.

$$y_c(x) = 4\delta\left(\frac{x}{c}\right)(c-x) \qquad \text{Eq. (8)}$$

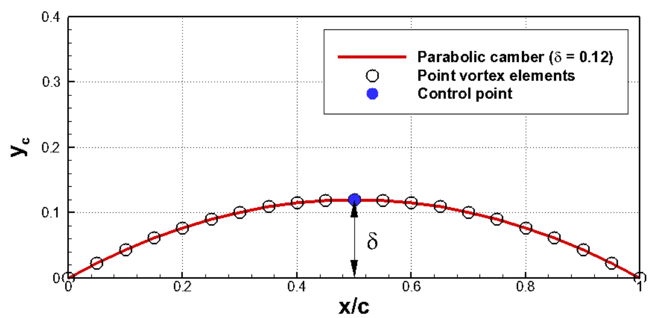

Fig. 2 Parabolic camber distribution

The induced velocity at an arbitrary control point due to M number of point vortex elements is written as in Eq. (9). The point vortex element with a strength of the circulation Γ_i is assigned corresponding to each vortex panel where i implies the index along the chordwise direction. x_{cp} and y_{cp} are the coordinates of the control point, x_i and y_i are the coordinates of the i-th point vortex, and r_i is the distance between the control point and i-th point vortex.

$$V_{cp} = \sum_{i=1}^{M} \frac{\Gamma_i}{2\pi r_i} = \sum_{i=1}^{M} \frac{\Gamma_i}{2\pi\sqrt{(x_{cp}-x_i)^2+(y_{cp}-y_i)^2}} \qquad \text{Eq. (9)}$$

In addition, the normal component of the free stream at the arbitrary control point is expressed as in Eq. (10), which can be approximated by a small angle assumption.

$$V_{\infty,n} = V_{\infty} \sin\left(\alpha + \tan^{-1}\left(-\frac{dy_c}{dx}\right)\right) \approx V_{\infty}\left(\alpha - \frac{dy_c}{dx}\right) \quad \text{Eq. (10)}$$

The zero normal flow boundary condition at the control point should be satisfied as follows:

$$\sum_{i=1}^{M} \frac{\Gamma_i}{2\pi\sqrt{(x_{cp}-x_i)^2+(y_{cp}-y_i)^2}} = V_{\infty}\left(\alpha - \frac{dy_c}{dx}\right) \quad \text{Eq. (11)}$$

To make use of the relation between the Kutta-Joukowski theorem and thin airfoil theory, the representative circulation strength (Γ_{avg}) is defined by averaging *M* circulation strengths of the chordwise vortex elements. Hence, the discretized vortex elements with individual circulation strength along the chordwise direction are regarded as only a single vortex element with averaged circulation strength. This assumption will be applied to the three-dimensional rotor blade. *M* chordwise vortex elements at each blade section are considered as an equivalent curved single vortex element placed on the camber surface, and its circulation strength is assumed to be equal to the averaged value of the chordwise circulation strength. Then, the relation between the expression for the lift force of the Kutta-Joukowski theorem and thin airfoil theory can be derived as in Eq. (12)

$$L = \rho_{\infty} V_{\infty} \Gamma_{avg} = \frac{1}{2}\rho_{\infty} V_{\infty}^2 2\pi\left(\alpha + 2\delta\right)c \quad \text{Eq. (12)}$$

Both Eq. (11) and Eq. (12) can be rearranged to obtain an expression for the freestream velocity, and the equation for unknown location of the control point (x_{cp}) is finally derived by combining them as shown in Eq. (13).

$$\frac{1}{\left(\alpha - \frac{dy_c}{dx}\right)} \sum_{i=1}^{M} \frac{\Gamma_i}{2\pi\sqrt{(x_{cp}-x_i)^2+(y_{cp}-y_i)^2}} = \frac{\Gamma_{avg}}{\pi\left(\alpha + 2\delta\right)c} \quad \text{Eq. (13)}$$

Assuming that the circulation distribution, maximum camber, and camber function are known, the equation for determining the location of the control point is numerically solved using the root finding approach. It was observed that the location of the control points converged into a half chord on the camber line by increasing the number of vortex elements. The location of the control points can be also determined for a symmetric airfoil in a similar manner. The results show that the most suitable location of the control point for NVLM is at half of the chord. The detailed derivation is out of the scope of the current study. For further information, refer to the reference [14].

2.2 Airfoil table look up

Once the strength of bound vortices on the rotor blade is determined by solving the linear system of equations with an instantaneous boundary condition at each time step, the resulting aerodynamic forces generated by the rotor blade can be calculated by using the Kutta-Joukowski theorem. However, the major shortcomings of using VLM are that the flow phenomena arising from the viscous and compressible effects cannot be inherently captured since it is based on assuming the incompressible linear potential theory. VLM especially fails to predict the nonlinear aerodynamic behaviors occurring in the stall and post-stall region, such as an abrupt drop in the lift coefficient. As a result, VLM tends to excessively over-predict the lift force and circulation strength. The look-up table is an efficient and practical way for obtaining the aerodynamic information of airfoils subjected to the attached and stalled flow. In the NVLM, the sectional look-up table was conducted to obtain the lift and drag coefficients at the control point of each blade section. For obtaining the aerodynamic coefficients, the local inflow velocity, inflow angle, and effective angle of attack were evaluated using Eq. (5), (6) and (7), respectively. Finally, the sectional lift forces generated by each blade section can be taken as in Eq. (14).

$$dL_{j,\text{table}} = \frac{1}{2}\rho_\infty \left((\mathbf{V}_{\text{inflow}} \cdot \mathbf{a}_1)^2 + (\mathbf{V}_{\text{inflow}} \cdot \mathbf{a}_3)^2 \right) c_{l,j} dA_j \qquad \text{Eq. (14)}$$

Since the two-dimensional airfoil table typically includes the aerodynamic coefficients for both pre and post-stall region, the NVLM can evaluate the aerodynamic performance of the rotor blades at below and above stall angles. The use of the two-dimensional aerodynamic coefficients table allows NVLM to consider the thickness, viscous and compressible effects.

2.3 Circulation strength correction

As mentioned before, since the table contains the aerodynamic coefficients in post-stall regions, the sectional lift force over stall onset angle can be estimated through the look-up table. However, the bound circulation strength on the rotor blades obtained from solving the linear system of the equation still could be largely over-estimated. In the vortex theory, the vortex elements placed on the trailing edge of rotor blades will shed into the wake and their strength remains constant by the Helmholtz's theorem. As a result, the over-predicted strength of bound and wake vortices could cause inaccurate wake geometry and induced velocity at the control points. Therefore, the influence of stalled flow on the circulation strength should be also included to obtain a more accurate solution. In the NVLM, the sectional lift forces obtained from the look-up table are used to correct the bound vortex strength computed from VLM. The representative circulation strength at the control point, denoted as $\Gamma_{\mathrm{table},j}$, can be newly computed by equating the expressions for the sectional lift forces as in Eq. (14) and the Kutta-Joukowski theorem. The circulation strength correction with an under-relaxation factor will iteratively be conducted until a convergence criterion is satisfied. If the difference between current and updated circulation strengths becomes within 0.001%, then the iterative correction will be stopped and the corrected circulation strength will be assigned into both the chordwise and the spanwise vortex elements depending on a strength ratio of each chordwise element strength to the averaged strength. A detailed description of the circulation strength correction procedure is discussed as follows and depicted in Fig. 3.

1. Obtain an initial circulation strength of vortex ring elements distributed on the blade by solving a linear system of equations $\Gamma_{i,j}$.
2. Assume that the representative circulation strength for each blade section is defined as an averaged circulation strength along with M chordwise elements. Define the strength ratio of each chordwise element strength to averaged strength, and it will be used to assign the corrected circulation strength to the chordwise circulation strength.

$$\Gamma_{\mathrm{avg},j} = \frac{1}{M}\sum_{i=1}^{M}\Gamma_{i,j}\ , \quad \lambda_{i,j} = \frac{\Gamma_{i,j}}{\Gamma_{\mathrm{avg},j}} \qquad \text{Eq. (15)}$$

3. For each blade section, compute the local inflow velocity ($\mathbf{V}_{\text{inflow}}$), inflow angle ($\alpha_{\text{inflow}}$) and effective angle of attack (α_{eff}) at the control points using Eq. (5), (6) and (7), respectively.
4. Obtain the lift (c_l) and drag (c_d) coefficients corresponding to the evaluated local inflow velocity and effective angle of attack through the look-up table.
5. Using the lift coefficients obtained from the look-up table in the step 4, a new circulation distribution in the spanwise direction ($\Gamma_{\text{table},j}$) can be calculated by matching the two equations representing sectional lift forces as in Eq. (14) and Eq. (16). The former equation is derived from the airfoil theory, while the later equation is associated with the Kutta-Joukowski theorem. [6]

$$dL = \rho_\infty \Gamma \sqrt{\left((\mathbf{V}_{\text{inflow}} \times d\,\mathbf{l})\cdot \mathbf{a}_1\right)^2 + \left((\mathbf{V}_{\text{inflow}} \times d\,\mathbf{l})\cdot \mathbf{a}_3\right)^2} \qquad \text{Eq. (16)}$$

$$\Gamma_{\text{table},j} = \frac{\frac{1}{2}\left((\mathbf{V}_{\text{inflow}}\cdot \mathbf{a}_1)^2 + (\mathbf{V}_{\text{inflow}}\cdot \mathbf{a}_3)^2\right) c_{l,j}\, dA_j}{\sqrt{\left((\mathbf{V}_{\text{inflow}} \times d\,\mathbf{l})\cdot \mathbf{a}_1\right)^2 + \left((\mathbf{V}_{\text{inflow}} \times d\,\mathbf{l})\cdot \mathbf{a}_3\right)^2}} \qquad \text{Eq. (17)}$$

6. Compare the newly evaluated circulation strength ($\Gamma_{\text{table},j}$) with initial circulation strength ($\Gamma_{\text{avg},j}$) obtained from step 1. If there is disparity between them, then the circulation strength is corrected with an under-relaxation factor, denoted as *D*.

$$\text{If} \quad k = 1, \;\; \Gamma_j^{k+1} = \Gamma_{\text{avg},j}^{k} + D(\Gamma_{\text{table},j}^{k} - \Gamma_{\text{avg},j}^{k}) \qquad \text{Eq. (18)}$$

$$\text{else} \;\; k \neq 1, \;\; \Gamma_j^{k+1} = \Gamma_{\text{table},j}^{k} + D(\Gamma_{\text{table},j}^{k} - \Gamma_{\text{table},j}^{k-1})$$

Note that *k* is the iteration step and *D* is a damping factor for the iterations. From our experience, the value of the damping factor is recommended from 0.05 to 0.1 in order to preserve the numerical stability.

7. Iteratively correct the circulation strength until a convergence criterion is satisfied. If the difference between current and updated circulation strengths becomes within 0.001%, then go to next step. Else, return to step 3.

8. Apply the updated circulation strength of each blade section into total $N \times M$ vortex ring elements using the strength ration defined in step 2, and the time-marching wake convection with updated circulation strength is conducted.

$$\Gamma_{i,j} = \Gamma_j^{k+1} \lambda_{i,j} \qquad \text{Eq. (19)}$$

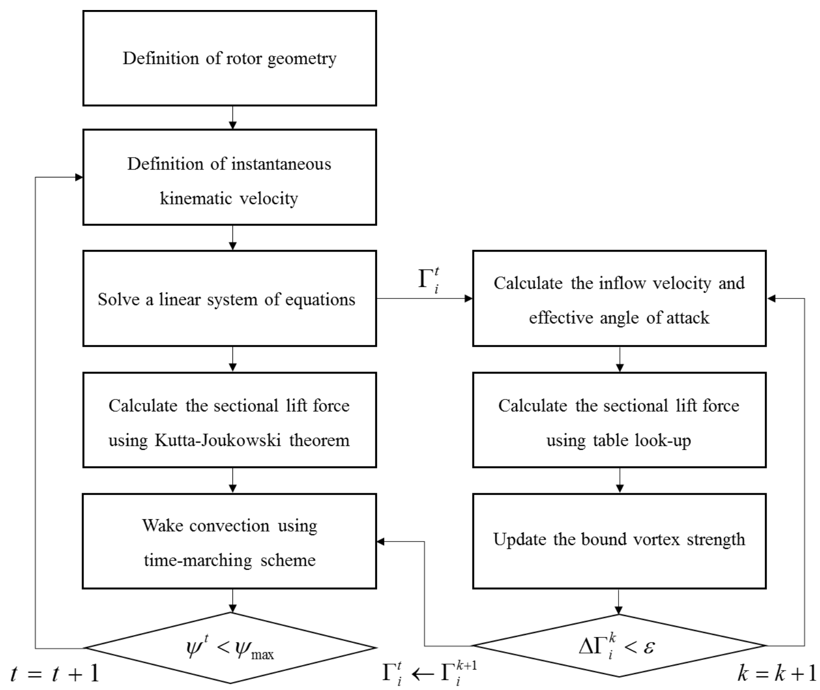

Fig. 3 Flowchart for nonlinear vortex lattice method

After several iterations, the bound circulation strength on the rotor blade converged. The corrected bound vortices located at the trailing edge will shed into the wake by applying the Kutta condition. For each time step, the rotor blade is rotated, and the wake vortex elements are generated from the trailing edge of the rotor blades. In the current study, the vortex particle method was employed to model the wind turbine wake. The detailed description of the vortex particle method will be discussed in the following section.

3. Numerical modeling

3.1 MEXICO wind turbine

The validation of the NVLM was conducted by comparing the predicted results with the MEXICO rotor measurements, including aerodynamic performance of the rotor blade and tip vortex geometry. The measurements on the MEXICO wind turbine with 4.5 m of three-bladed rotors have been performed at the German-Dutch Wind Tunnels (DNW) facilities. The rotor configuration is upwind type without hub tilt, coning, and prebend angles. The pitch angle of the blade is -2.3° where the negative sign implies that the airfoils rotate in the feathering direction. The rotor blade is composed of the three different airfoils: DU91-W2-250 airfoil at the inboard of the blade, RISØ-A1-21 airfoil at the mid-span of the blade, and NACA64-418 airfoil at the outboard of the blade. The rotor blade has a tapered-twisted planform shape as depicted in Fig. 4 [15, 16]. The MEXICO rotor mode was subjected to 10, 15, and 24 m/s of the incoming wind speeds corresponding to turbulent wake state, design condition and separated flow condition, while the rotor speed remained approximately constant at 425.1 rpm, as listed in Table 1.

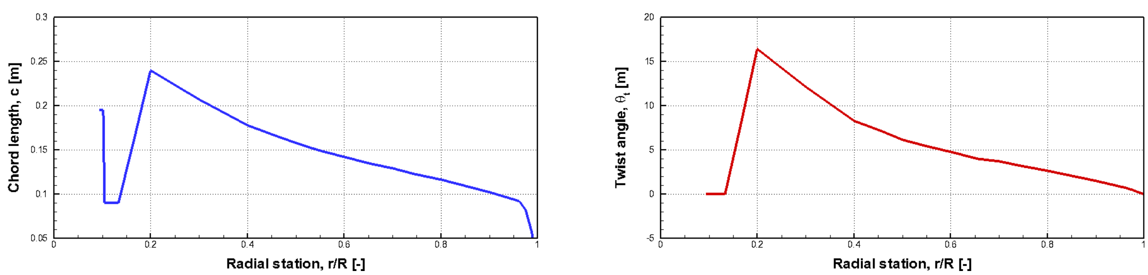

(a) Chord distribution of MEXICO rotor blade (b) Twist angle distribution of MEXICO rotor blade

Fig. 4 Chord (a) and twist angle (b) distribution along the span of the blade

Table 1. Description of measurement conditions

Case	Wind speed [m/s]	Rotor speed [rpm]	TSR [-]	Density [kg/m^3]
1	10.05	425.1	10.02	1.197
2	15.06	425.1	6.68	1.191
3	24.05	425.1	4.17	1.195

3.2 Blade and wake model

As aforementioned, the MEXICO rotor model has the tapered-twisted planform shape with three different airfoils. The quadrilateral vortex elements along the chordwise and spanwise directions are used to model the rotor blades, and they are placed on the camber surface of the blade to geometrically represent a curvature of the blade surface. The grid resolution is one of the important factors that determine the accuracy and efficiency of the numerical simulation. A sufficiently fine grid resolution is needed to capture the large gradient of aerodynamic loads and vorticity along the spanwise direction at the particular root and tip sections. Each one of the rotor blades was discretized by using 15×30 vortex ring elements with a dense distribution in the root and tip locations as shown in Fig. 5. The required information for blade modeling, including planform shapes and airfoil coordinates, are provided from references [16].

In the present paper, the rotor wake is shed from a full span of the rotor blade, and its geometry is modeled by means of two approaches: curved vortex filaments and vortex particles. As shown in Fig. 5, the nascent wake that recently shed from the full span of the blades is represented using the curved vortex filaments during approximately 4-5 discretized time steps. After that, the vortex filaments are split into a finite number of vortex particles except for the nascent wake panels. The strength of vortex particles has been already determined at the previous time step by imposing Kutta condition at the trailing edge panels. During time-marching step, vortex particles that mutually interact with each other are allowed to freely distort and naturally move toward downstream. A numerical time integration scheme is required to update the positions of the vortex particle at each time step, and it plays an important role in the accuracy and stability of the wake geometry and the vorticity field behind the rotor blade. The second order Runge-Kutta method was used here. The time step size for the wake convection is also an important factor. Although the smaller time step size can yield better accurate solutions, this will demand significantly large computational time. In the current study, the wind turbine was exposed to an axial flow condition where the incoming wind direction was aligned with the rotating axis of the rotor blade. The hub tilt angle of the MEXICO rotor model is also zero. Therefore, the aerodynamic loads on the blade are symmetrically generated with respect to the azimuth angles and the helical wake geometry is convected into downstream without skewness. Therefore, a discretization of the time step $\Delta\psi = 10°$ has been used. It was observed that this value can efficiently provide accurate solutions for the axial flow condition. It should be also noted that the initial wake state affects the numerical instability and convergence of the wake geometries in the time marching method [17, 18]. To avoid the numerical problems occurring in the wake simulation, the rotational speed of the rotor blade was slowly increased from zero to the required speed, instead of an impulsive increase of the rotational speed. The numerical simulation was carried out for a total of 12 revolutions with 1 revolution of slow starting rotation, which are enough to obtain a converged solution of aerodynamic performances, wake structure, and vorticity field.

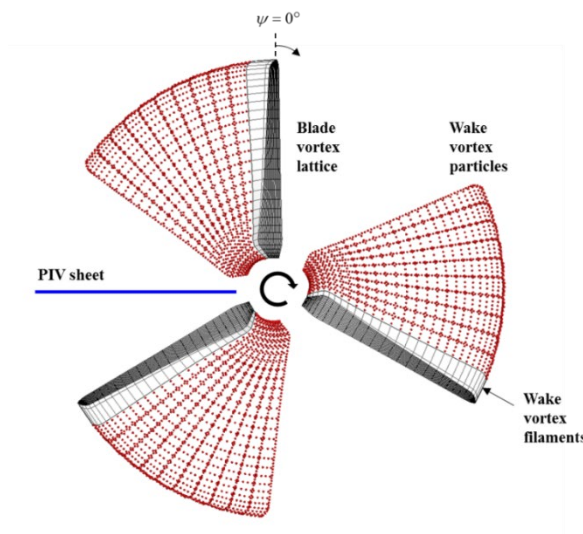

Fig. 5 Rotor blade and wake modeling

3.3 Airfoil table and stall delay model

The two-dimensional aerodynamic coefficient data were required to conduct the look-up table for NVLM simulation, and their quality play important roles in determining the accuracy of NVLM results. The MEXICO rotor blade is composed of three different airfoils including the DU91-W2-250, the RISØ-A1-21, and the NACA 64-418 airfoils. Their lift and drag coefficients with respect to the angle of attack including pre-stall and post-stall regions are obtained from references [16], as depicted in Fig 6. DU and NACA airfoils have been the subject of measurement in the Delft University wind tunnel (LST) facility [24, 25], while the aerodynamic coefficients of RISØ airfoil have been measured in the Velux wind tunnel at RISØ national laboratory in Denmark [26]. As demonstrated by the experiments, the centrifugal and Coriolis forces induced by the three-dimensional and rotational effects affect the stability of the boundary layer on rotating blades and can cause considerably increased lift coefficients compared to the corresponding two-dimensional or non-rotating case. These behaviors are referred to as stall delay phenomena or rotational augmentation. Several stall delay models have been developed to adjust the two-dimensional aerodynamic coefficients data to account for the three-dimensional rotational effect. In the present research, the Raj and Selig model [19] was used to take into account the effect of stall delay on the aerodynamic coefficients at the inboard section of the rotor blade. This model is based on an improvement of the Du and Selig model [20], which is derived from the analysis of the three-dimensional boundary layer equations on the rotating blade. The evident modification of the Raj and Selig model is that it includes an increase of the drag coefficient as well as an increase of the lift coefficient, as opposed to the decrease of the drag coefficient present in the Du and Selig model.

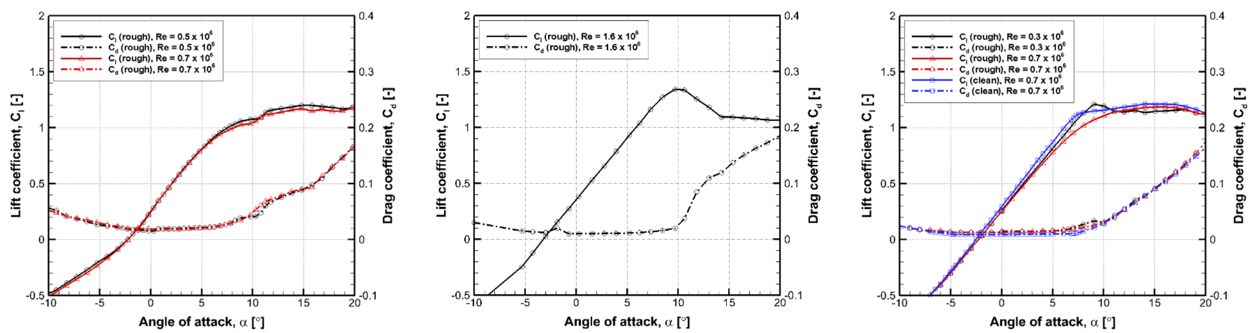

(a) DU91-W2-250 (b) RISØ-A1-21 (c) NACA 64-418

Fig. 6 Measured lift and drag coefficients of the airfoils used in the MEXICO blades

4. Results and discussion

4.1 Aerodynamic loads

The aerodynamic performance of the wind turbine under axial flow conditions with three different wind speeds was numerically calculated using the NVLM method, and the results were compared with the predicted and measured data. A model comparison was conducted with the numerical solutions computed by LLM [21], actuator disk model (ADM) [22], and RANS [23]. LLM is based on the generalized Prandtl lifting line theory and the shed wake is modeled using the free-wake vortex filament method. In the LLM simulation, the blade surface does not have to be modeled because it is represented by the concentrated vortex line. ADM simulation used the multi-block finite volume Navier-Stokes solver in conjunction with the actuator disc techniques. The rotor blade was replaced by the body forces distributed over a disc. The EllipSys3D incompressible CFD solver was also used for RANS simulation with Menter's $k - \omega$ SST turbulence model.

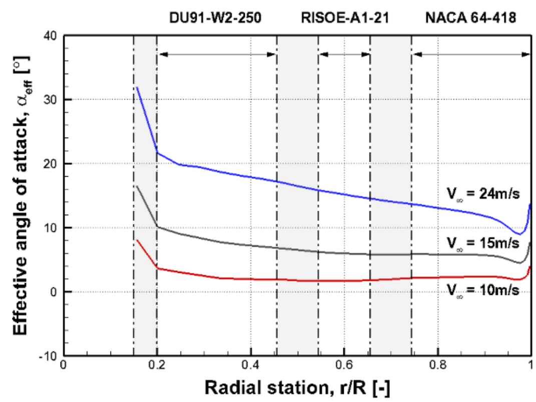

Fig. 7 Effective angle of attack distribution in the spanwise direction

The local effective angle of attack at each blade section was directly determined depending on the incoming wind speed as shown in Fig. 7. In wind turbine aerodynamics, when the incoming wind speed increases, the inflow angle and angle of attack increase under the controlled pitch and rotating speed conditions. In the case of the wind speed of 24 m/s, it is observed that the distribution of the effective angle of attack along the radial direction is mostly greater than the stall onset angles. Therefore, this wind speed corresponds to the separation flow condition in which the boundary layer on the upper surface of the airfoil is finally separated.

At a wind speed of 10 m/s, the wind turbine is subjected to the turbulent wake state condition. It is observed that the strong interaction between tip and root wake vortices and a highly unsteady wake structure took place in the downstream. The details of the wake geometry and vorticity field are further discussed in the following section. The comparison of the normal and tangential forces that is normal and tangential to the reference frame of chord line is shown in Fig. 8. The computed normal forces generally agree well with the measured data. However, the tangential force distributions computed by LLM, ADM, and RANS do not well match with the experiments, while the agreement for the results of NVLM remains quite good as indicated in Fig. 8(b). Especially, the considerable over-prediction in the tangential force can be observed in the ADM results. It could be inferred that the limitation of geometric blade modeling and numerical dissipation error in the vorticity field are found to be responsible for the discrepancy with the measured data. LLM also fails to predict the tangential force at a particular mid-section of the rotor blade due to the limitation of the blade modeling because the prediction of tangential force could be largely influenced by a curvature of the lifting body. Compared to other approaches, the overall differences in the normal and tangential forces between NVLM results and measurements are quite small. It indicates that the complicated circular wake patterns could be well described and their influences accurately are considered to evaluate the aerodynamic loads acting on the rotor blades.

The comparison results for the wind speed of 15 m/s are shown in Fig. 9. The incoming wind speed of 15 m/s is the design condition of the MEXICO wind turbine. Unlike the turbulent wake state, the helical wake geometry will be generated and transported toward downstream without the strong wake interaction. These can be clearly confirmed in the following section. As indicated in Fig. 9(a), all numerical methods provided quite accurate solutions for predicting normal force distributions. However, there is some discrepancy in the tangential force distributions between the predicted results and measurements. Although the tangential load distributions computed by LLM and ADM are generally in agreement with measurements near the inboard sections, they tend to over predict the tangential load distribution at the mid-span of the rotor blade. NVLM results showed that the proposed method yielded the most accurate results from mid-span to the tip section of the rotor blade. The tangential forces are slightly under-estimated at only the inboard section due to a lack of hub modeling. Consequently, it is evident that the NVLM can achieve better solutions for the prediction in both normal and tangential forces compared with other approaches.

For the MEXICO wind turbine, the wind speed of 24 m/s corresponds to the separation flow condition. The comparison results for the wind speed of 24 m/s are shown in Fig. 10. The radial distribution of normal forces computed by NVLM is well matched with the experiments except at 0.82 R and 0.92 R radial positions. It can be observed that the proposed method is able to capture the effect of the stalled flow. In addition, the computed tangential loads are much closer to the experiment than the results from LLM and ADM. An apparent discrepancy with measurements can be observed in the results of LLM and ADM simulations that yielded a considerable under-prediction in the normal and tangential forces. Although the LLM simulation could yield a reasonably accurate solution for the distribution of normal force, a large discrepancy in the predicted tangential force distribution was observed for all three wind conditions. It might be attributed to the shortcoming of blade surface modeling. The differences in the aerodynamic forces between ADM and NVLM are pronounced at the inboard locations. It seems possible that the different results were caused by the use of the stall delay model. ADM used only two-dimensional aerodynamic data without the stall delay model, while the Raj and Selig stall delay model was employed to correct the three-dimensional rotational effects in NVLM simulation. RANS results showed that aerodynamic forces are generally over-predicted compared to measurements. This over-estimation could have a bearing on the turbulence model and numerical dissipation error occurring on the separated flow.

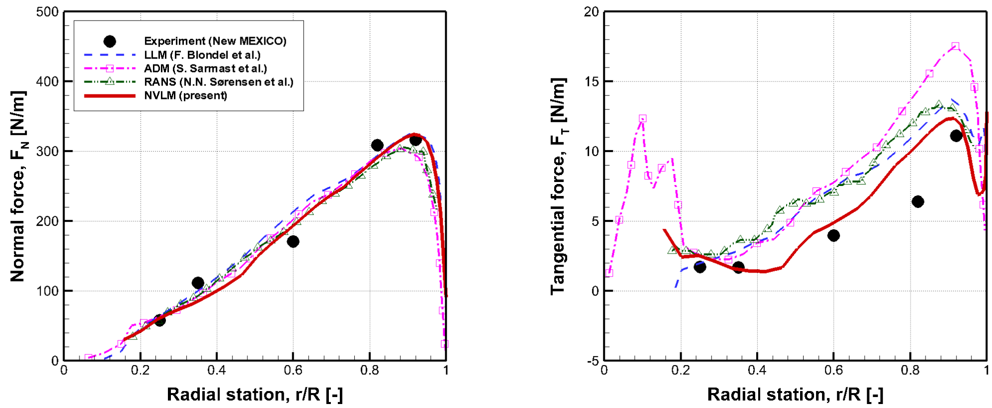

(a) Normal force (b) Tangential force

Fig. 8 Comparison of normal (left) and tangential (right) force at wind speed of 10 m/s

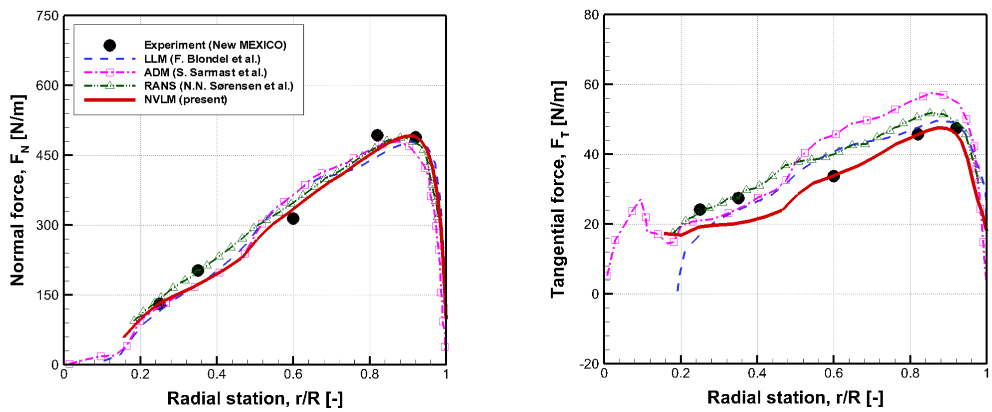

(a) Normal force (b) Tangential force

Fig. 9 Comparison of normal (left) and tangential (right) force at wind speed of 15 m/s

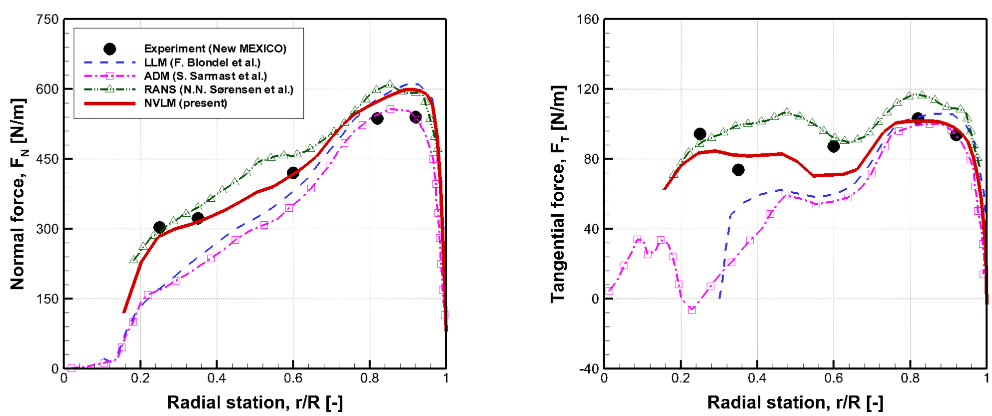

(a) Normal force (b) Tangential force

Fig. 10 Comparison of normal (left) and tangential (right) force at wind speed of 24 m/s

4.2 Wake structure

In wind turbine aerodynamics, the wake expansion angle and pitch length play an important role in determining the aerodynamic performance of wind turbine. Therefore, it is important to accurately track the tip vortex trajectories with respect to time. In the present research, the wake geometries generated by a three-bladed rotor were numerically predicted using the time-marching vortex particle method. The accuracy of wake modeling can be verified against measured locations of tip vortex in terms of the radial and axial positions. In the MEXICO project, the tip vortex positions were measured by a particle image velocimetry (PIV) sheet located horizontally in the x-z plane where the azimuth angle is 270°, as shown in Fig. 5.

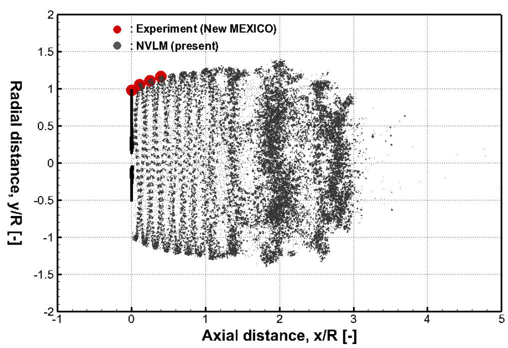

(a) Wind speed V_∞ = 10 m/s

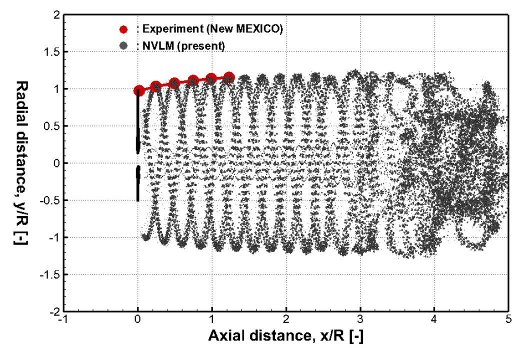

(b) Wind speed V_∞ = 15 m/s

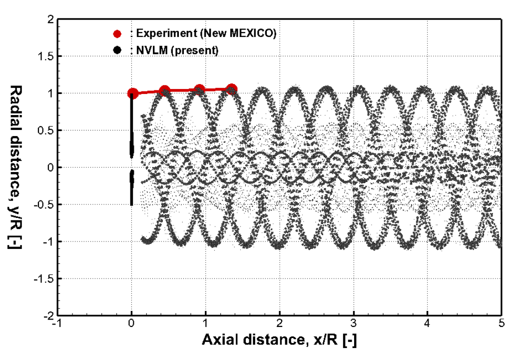

(c) Wind speed V_∞ = 24 m/s

Fig. 11 Comparison of tip vortex trajectory depending on wind speeds

The well-defined tip vortex geometries originating from the three-bladed rotor can be captured depending on the incoming wind speeds. as depicted in Fig. 11. The comparison showed excellent agreement in both axial and radial positions with measurements for all wind conditions. For higher wind speeds, the wake geometries become stable, the radial positions of the tip vortex contract and the axial positions of the tip vortex increase. In other words, the wake expansion angles reduce, and the tip vortex pitch increases as the wind speed increases. The tip vortex pitch is the distance along the axial direction between two successive tip vortex cores shed from the same rotor blade. As a result, the overall agreement in the tip vortex geometries obtained with the NVLM is quite good when the rotor blades are exposed to the separation flow condition as well as the turbulent wake state. These comparison results have been employed to prove that the implemented time-accurate vortex particle method is capable of accurately capturing the wake geometries of the wind turbine subjected to various wind conditions.

Fig. 12, 13 and 14 showed the time-accurate solutions of the rotor wake structure and vorticity contour with respect to the number of rotor revolutions. The color of the vortex particles implies their vortex strength. The particles with strong strength were assigned red color, while the particles with weak strength were assigned green color. For an incoming wind speed of 10 m/s, the rotor blades experience the turbulent wake state and a circular wake pattern is developed in the flow field behind the rotors. It is observed that a significant flow recirculation region and strong mixing region exist in the wake; it is similar to the turbulent wake of a bluff body. As illustrated in Fig. 12, the tip and root vortices move radially inward and outward, respectively. Afterwards, they begin to strongly interact with each other and merge to form the mixing vortices. Consequently, the helical wake geometry completely breaks down in the downstream. This is called tip vortex breakdown phenomenon. At the low wind speed condition (high tip speed ratio) corresponding to the turbulent wake or vortex ring state, BEM is prone to cause a numerical convergence problem because the underlying assumption for momentum theory breaks down. On the other hand, the NVLM can be employed to simulate the wind turbine for a wide range of operating conditions. For wind speeds of 15 and 24 m/s, high strength of the tip vortices is captured as shown in Fig. 13 and 14, respectively. Unlike the turbulent wake state, the wake geometry becomes stable and the helical structure maintains further downstream without the strong wake-wake interaction owing to the high convection velocity of wake vortices.

When the flow separation massively occurs from the upper surface of the airfoil, the vorticity field computed by NVLM could not rigorously match with the actual vorticity field due to lack of an additional wake model for separated flow. Although the aerodynamic loads and circulation strength are correct to consider the influence of stalled flow, the separated flow from the upper surface of the rotor blade is not explicitly modeled. Therefore, an additional wake model for separated flow is needed to resolve this limitation.

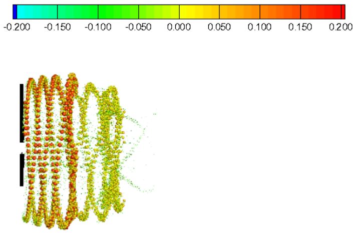

(a) Wake vortex particles at 4 revolutions

(b) Vorticity contour at 4 revolutions

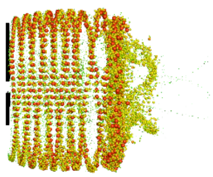

(c) Wake vortex particles at 6 revolutions

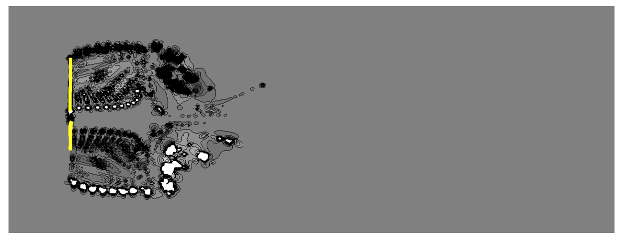

(d) Vorticity contour at 6 revolutions

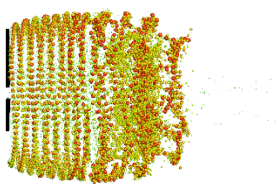

(e) Wake vortex particles at 8 revolutions

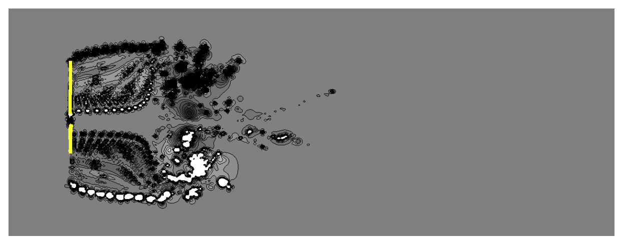

(f) Vorticity contour at 8 revolutions

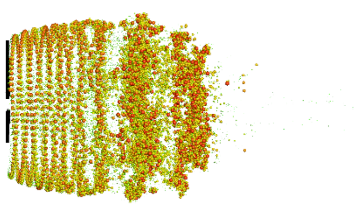

(g) Wake vortex particles at 10 revolutions

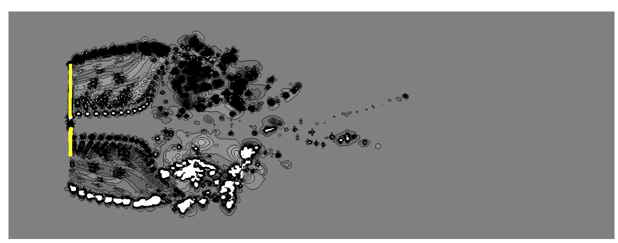

(h) Vorticity contour at 10 revolutions

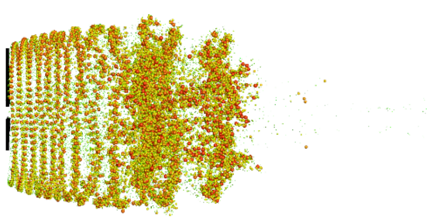

(i) Wake vortex particles at 12 revolutions

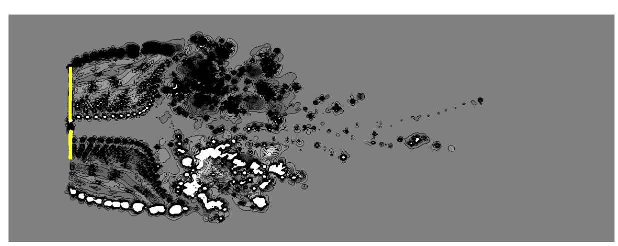

(j) Vorticity contour at 12 revolutions

Fig. 12 Evolution of wake geometries and vortices at wind speed of 10 m/s

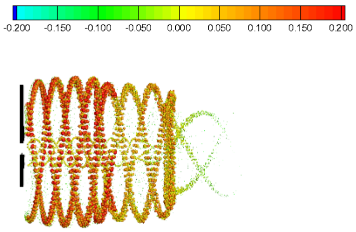

(a) Wake vortex particles at 4 revolutions

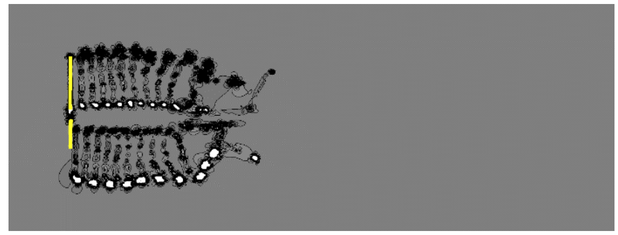

(b) Vorticity contour at 4 revolutions

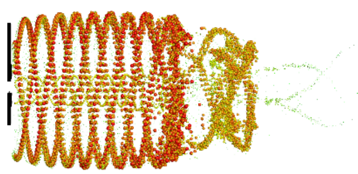

(c) Wake vortex particles at 6 revolutions

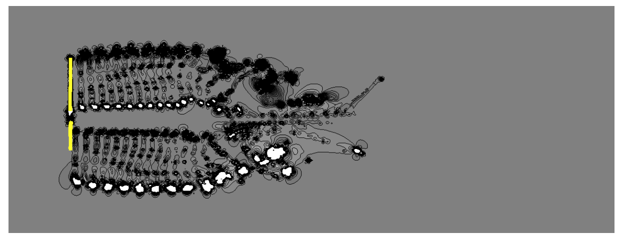

(d) Vorticity contour at 6 revolutions

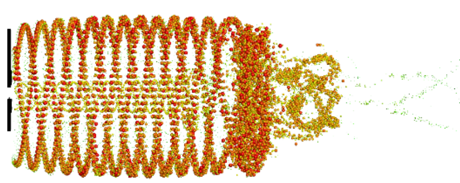

(e) Wake vortex particles at 8 revolutions

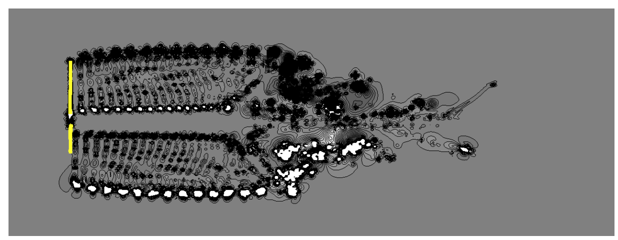

(f) Vorticity contour at 8 revolutions

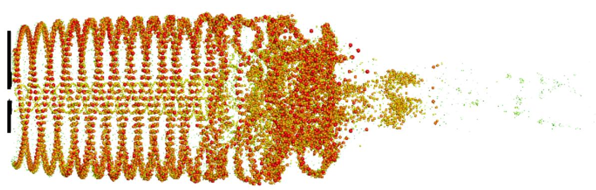

(g) Wake vortex particles at 10 revolutions

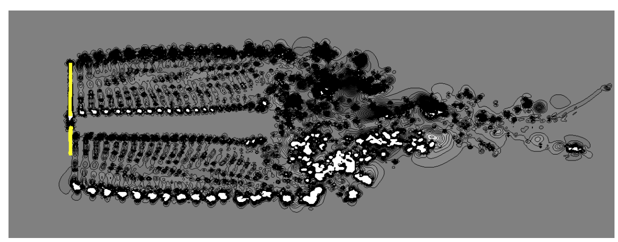

(h) Vorticity contour at 10 revolutions

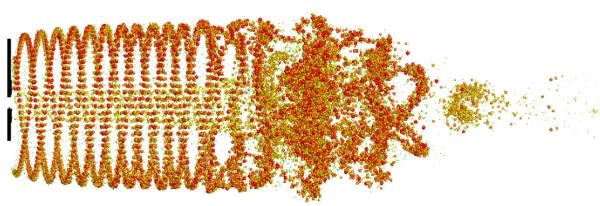

(i) Wake vortex particles at 12 revolutions

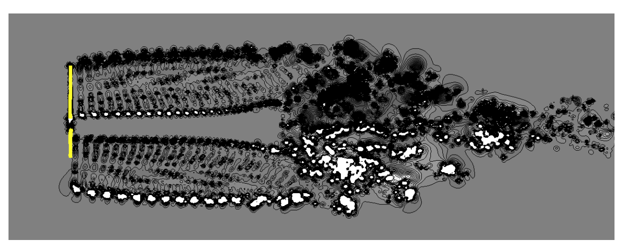

(j) Vorticity contour at 12 revolutions

Fig. 13 Evolution of wake geometries and vortices at wind speed of 15 m/s

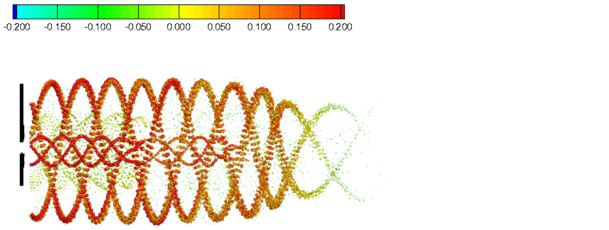

(a) Wake vortex particles at 4 revolutions

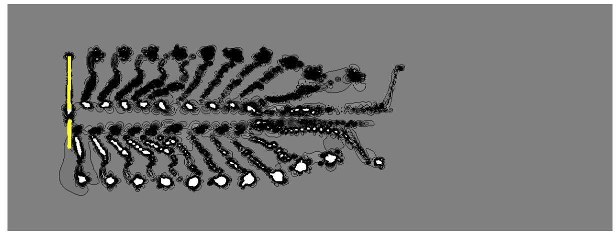

(b) Vorticity contour at 4 revolutions

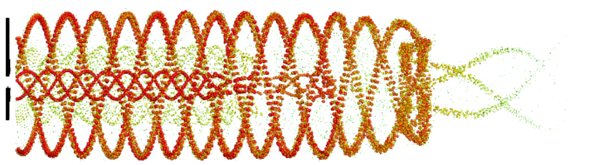

(c) Wake vortex particles at 6 revolutions

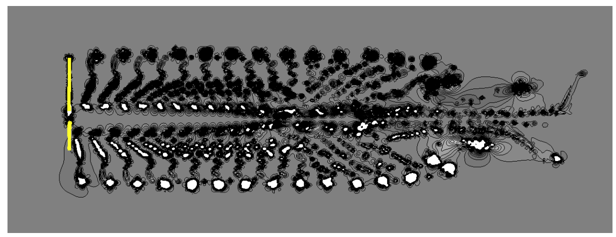

(d) Vorticity contour at 6 revolutions

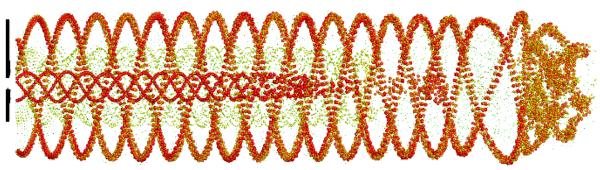

(e) Wake vortex particles at 8 revolutions

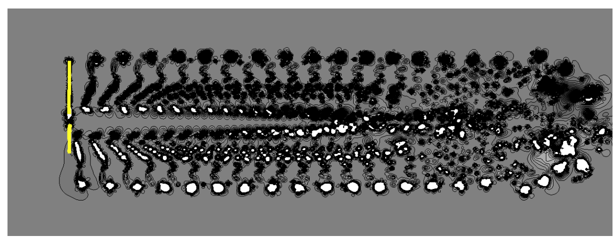

(f) Vorticity contour at 8 revolutions

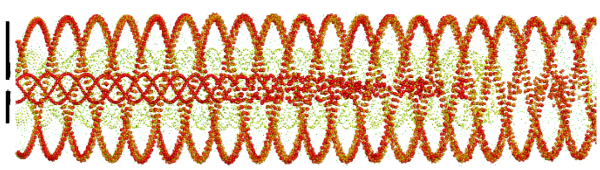

(g) Wake vortex particles at 10 revolutions

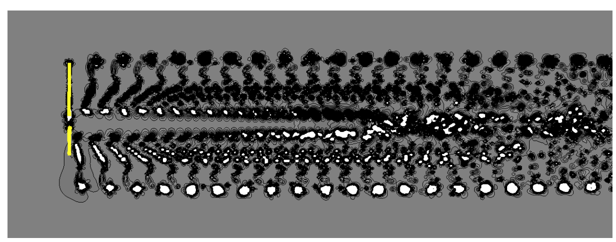

(h) Vorticity contour at 10 revolutions

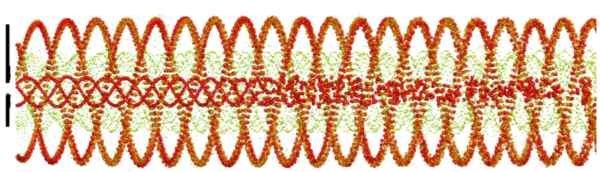

(i) Wake vortex particles at 12 revolutions

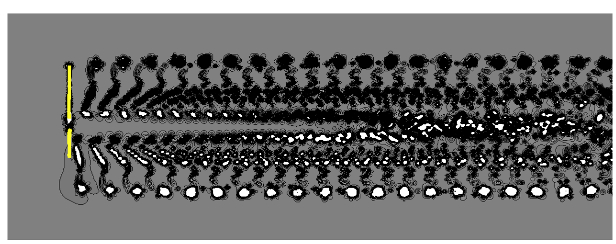

(j) Vorticity contour at 12 revolutions

Fig. 14 Evolution of wake geometries and vortices at wind speed of 24 m/s

5. Conclusion

The accurate prediction of aerodynamic performance is considerably important for the efficient and reliable design of wind turbine blades. Among several numerical models, the vortex lattice method (VLM) is widely used for comprehensive analysis of wind turbines because it demands low computational cost and provides a reasonably accurate solution for the subsonic flow. In the present research, the approach for extending VLM to take into account the effect of the nonlinear stall and post-stall flow has been suggested. It is referred as the nonlinear vortex lattice method (NVLM), which incorporates the airfoil look-up table and iterative circulation strength correction. The effective angle of attack should be evaluated at the control points for conducting look-up table, hence their location was found by applying the zero normal boundary condition to the VLM. It was found that the most suitable location for NVLM was the half chord of the camber line. Model validation was conducted against high-quality measurements on the MEXICO rotor model under axial flow with three different wind conditions. The comparison showed that the aerodynamic loads computed by NVLM were well matched with the measurements and the NVLM was able to achieve better solutions compared to other methods even if the flow separation occurs from the rotor blades. It indicated that the proposed method is capable of predicting the nonlinear aerodynamic characteristics resulting from stalled flow. In addition, the tip vortex trajectories in terms of the radial and axial positions calculated by NVLM are in significantly good agreement with the measurements for all wind conditions.

In the current study, the complicated wake structures, including the helical evolution patterns and tip vortex breakdown are clearly captured by using the vortex particle method. This provides a scope for further research to investigate the unsteady wake dynamics of the wind turbine under yawed flow conditions. When the yaw misalignment is present, a skewed wake structure will be developed that causes the strong wake-wake interaction, an asymmetric inflow distribution on the rotor blades and the azimuthal variations in aerodynamic loading. The proposed method will be useful to analyze the unsteady aerodynamic characteristics of the yawed rotor configuration since it can incorporate the dynamic stall models. The numerical investigation of the wind turbine under non-axial flow condition will be carried out in the future works.

Declaration of interest

There is no conflict of interest

Acknowledgments

The data used have been supplied by the consortium which carried out the EU FP5 project Mexico: 'Model rotor EXperiments In COntrolled conditions'. The consortium received additional support to perform the New Mexico measurements from the EU projects ESWIRP and INNWIND.EU. This research was supported by the Climate Change Research Hub of KAIST (Grant No. N11180110). This work was also supported by the Korea Institute of Energy Technology Evaluation and Planning (KETEP) and the Ministry of Trade, Industry & Energy (MOTIE) of the Republic of Korea (No. 20168520021200)

References

[1] Anderson, J.D., Corda, S., and van Wie, D.M., “Numerical Lifting Line Theory Applied to Drooped Leading-Edge Wings Below and Above Stall,” *Journal of Aircraft*, 17(12), 1980, pp. 898-904.

[2] Owens, D.B., “Weissinger’s model of the nonlinear lifting-line method for aircraft design,” *36th AIAA Aerospace Science Meeting and Exhibit*, Reno, Nevada, AIAA 98-0597,1998.

[3] Gupta, S., “Development of a time-accurate viscous lagrangian vortex wake model for wind turbine applications,” Ph.D. Thesis, University of Maryland, 2006.

[4] Gupta, S., and Leishman, J.G., “Performance predictions of the NREL Phase VI combined experiment rotor using a free-vortex wake model,” *44th AIAA Aerospace Sciences Meeting and Exhibit*, Reno, Nevada, AIAA 2006-390, 2006.

[5] Duque, E. P. N., Burklund, M. D., and Johnson, W., “Navier-Stokes and Comprehensive Analysis Performance Predictions of the NREL Phase VI Experiment,” *Journal of Solar Energy Engineering*, 125(4), 2003, pp. 457-467.

[6] van Garrel, A., “Development of a Wind Turbine Aerodynamics Simulation Module,” ECN-C-03-079, 2003

[7] Gaertner, E.M., “Modeling Dynamic Stall for a Free Vortex Wake Model of a Floating Offshore Wind Turbine,” M.S. Thesis, University of Massachusetts Amherst, 2014.

[8] Mukherjee, R., and Gopalarathnam, A., "Poststall Prediction of Multiple-Lifting-Surface Configurations Using a Decambering Approach," *Journal of Aircraft*, 43(3), 2006, pp. 660-668.

[9] Gopalarathnam, A., and Segawa, H., "Use of Lift Superposition for Improved Computational Efficiency of Wing Post-Stall Prediction," *26th AIAA Applied Aerodynamics Conference*, AIAA 2008-7049, 2008.

[10] Paul, R. C., and Gopalarathnam, A., "Iteration Schemes for Rapid Post-Stall Aerodynamic Prediction of Wings Using a Decambering Approach," *International Journal for Numerical Methods in Fluids*, 76(4), 2014, pp. 199-222.

[11] Santos, C. R. dos, and Marques, F. D., "Lift Prediction Including Stall, Using Vortex Lattice Method With Kirchhoff-Based Correction," *Journal of Aircraft*, 55(2), 2018. pp. 887-891.

[12] Abedi, H., Davidson, L., and Voutsinas, S., "Enhancement of Free Vortex Filament Method for Aerodynamic Loads on Rotor Blades," *Journal of Solar Energy Engineering,* 139(3), 2017, pp. 031007.

[13] Kim, H., Lee, S., and Lee, S., "Numerical analysis on the aerodynamics of HAWTs using nonlinear vortex strength correction," *Current Applied Physics*, 10, 2010, pp. S311-S315.

[14] Jo, Y.M., Lee, H.J., and Lee, D.J., "Prediction of Rotor Flow for Unmanned Aerial System Using Nonlinear Vortex Lattice Method," *6th Asian/Australian Rotorcraft Forum and Heli Japan 2017*, Kanazawa, Japan, 2017.

[15] Schepers, J.G., Boorsma, K., Cho, T., Gomez-Iradi, S., Schaffarczyk, P., Jeromin, A., Shen, W.Z., Lutz, T., Meister, K., Stoevesandt, B., Schreck, S., Micallef, D., Pereira, R., Sant, T., Madsen, H.A., and Sørensen, N., "Final report of IEA Task 29, Mexnext (Phase 1): Analysis of Mexico wind tunnel measurements," Technical Report, ECN-E12-004, Energy Research Center of the Netherlands, 2012.

[16] Schepers, J.G., Boorsma, K., Gomez-Iradi, S., Schaffarczyk, P., Madsen, H.A., and Sørensen, N.N., Shen, W.Z., Lutz, T., Schulz, C., Herraez, I. and Schreck, S., "Final report of IEA Wind Task 29: Mexnext (Phase 2), Technical Report, ECN-E—14-060, Energy Research Center of the Netherlands, 2014.

[17] Lee, D.J., and NA, S.U., "High resolution free vortex blob method for highly distorted vortex wake generated from a slowly starting rotor blade in hover," *Twenty-First European Rotorcraft Forum*, Paper No. II-5, Saint-Petersburg, Russia, 1995.

[18] Lee, D.J., and Na, S.U., "Numerical simulations of wake structure generated by rotating blades using a time marching, free vortex blob method," *European Journal of Mechanics-B/Fluids*, 18(1), 1999, pp. 147–159.

[19] Raj, N.V., "An improved semi-empirical model for 3-D post-stall effects in horizontal axis wind turbines," M.S. Thesis, University of Illinois, Urbana-Champaign, 2000.

[20] Du, Z. and Selig, M.S., "A 3-D stall-delay model for horizontal axis wind turbine performance prediction," *ASME Wind Energy Symposium, Aerospace Sciences Meeting,* AIAA-98-0021, 1998.

[21] Blondel, F., Boisard, B., Milekovic, M., Ferrer, G., Lienard, C. and Teixeira, D., "Validation and comparison of aerodynamic modelling approaches for wind turbines," *Journal of Physics: Conference Series*, 723, 2016, pp. 022029.

[22] Samast, S., Shen, W.Z., Zhu, W.J., Mikkelsen, R.F., Breton, S.P. and Ivanell, S., "Validation of the actuator line and disc techniques using the New MEXICO measurements," *Journal of Physics: Conference Series*, 723, 2016, pp. 032026.

[23] Sørensen, N.N., Zahle, F., Boorsma, K. and Schepers, G., "CFD computations of the second round of MEXICO rotor measurements," *Journal of Physics: Conference Series*, 753, 2016, pp. 022054.

[24] Timmer, W.A., Van Rooij, R.P.J.O.M., "Thick airfoils for HAWTs," *Journal of Wind Engineering and Industrial Aerodynamics*, 39, 1992, pp. 151-160.

[25] Timmer, W.A., Van Rooij, R.P.J.O.M., "Summary of the Delft University Wind Turbine Dedicated Airfoils." Journal of Solar Energy Engineering, 125(4), 2003. pp. 486-496.

[26] Fuglsang, P. and Bak, C., "Development of the Risø Wind Turbine Airfoils," *Wind Energy*, 7(2), 2004, pp. 145-162.